Heat exchanger integration with an aero-engine bypass duct

Raul Bajimaya[1], David MacManus[1], Chawki Abdessemed[1], Ioannis Goulos[1], Jesús Matesanz García[1], Christopher Sheaf[2], Vasileios Kyritsis[2]*

1 Centre of Propulsion and Thermal Power Engineering, School of Aerospace, Transport and Manufacturing, Cranfield University, Bedfordshire, United Kingdom, MK43 0AL

2 Rolls-Royce plc., P.O. box 31, Derby, United Kingdom, DE24 8BJ

First Author e-mail : Raul.bajimaya@cranfield.ac.uk

Abstract

The development of aero engines with geared fans may require the use of a heat exchanger system embedded within the bypass duct to dissipate heat due to the losses within the power gearbox of the fan. It is pertinent that the naturally ventilated heat exchanger system (HEX) is designed and installed to minimise detrimental impacts on the performance of the engine while meeting the HEX heat transfer requirements. This paper demonstrates the capabilities of a coupled mixed fidelity method to model a ventilated HEX embedded within the bypass duct. A systematic approach is presented to quantify the sensitivity of HEX heat transfer, HEX volume and engine net thrust to perturbation in HEX overall size and integration. A method to explore and quantify the trade-offs in HEX performance and bypass performance is detailed. The method can be used to allow rapid assessment of the integration of the HEX with the bypass duct.

1. Introduction

1.1 Background

The requirement to reduce the environmental effect of aviation has led manufacturers to the design and development of Ultra-High Bypass Ratio (UHBR) aero-engines with geared fans [1]. The heat losses within the power gearbox [2][3] introduces a challenge in the form of thermal management of the engine gearbox system [4]. The thermal management system can include the oil circuit for the power gearbox where the oil functions as a lubricant and a coolant simultaneously. Heat transferred from the gearbox components to the oil needs to be dissipated. This can potentially be achieved through the integration of an air-to-oil heat exchanger (HEX) [5] embedded into the bypass duct of the engine (Fig. 1). This allows the heat within the oil to be rejected into the bypass duct. The introduction of a HEX system will introduce a pressure drop and a temperature rise within the bypass duct. The benefitial effects of heat addition are likely to be negligible compared to the penalty due to the pressure loss [4]. Therefore it is essential to design and integrate HEX systems which minimize the detrimental impacts on the bypass performance while ensuring the HEX heat transfer requirements are met.

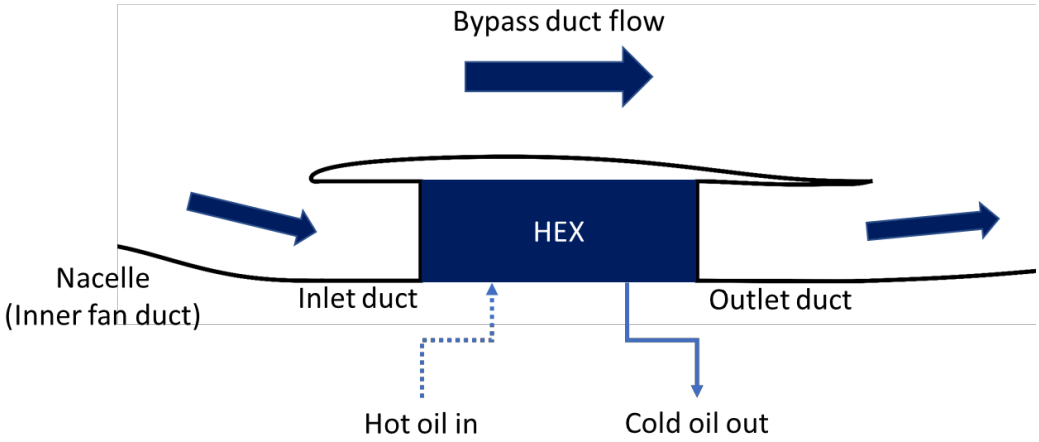

Figure 1 Schematic of a ventilated HEX system embedded in the bypass duct.

1.2 Scope

This paper demonstrates the capabilities of a coupled mixed fidelity method to model a ventilated HEX embedded within the bypass duct. The in-house tool GEMINI (Geometric Engine Modeler Including Nozzle Installation) was used to conduct aerothermal analysis of a ventilated, embedded HEX system integrated in the bypass duct of an aero-engine [6]. The tool is capable of parametrically producing engine and embedded HEX geometries. A mixed fidelity method was used to integrate a low order HEX model within a CFD solver [7]. This was done to avoid the development of a detailed HEX CFD model and thereby reduce computational load and allows more rapid design analyses. A heat exchanger design and modelling tool was used to generate HEX performance maps to be integrated into the low order HEX model [8]. The thrust-drag bookkeeping (TDB) method was used to quantify the effect of HEX system intergation on the aerodynamic performance of the bypass duct [9, 10, 11, 12].

The combined tools and methods were used to conduct design sensitivity analyses on the effects of HEX size and system immersion on bypass and HEX performance. The effect of systematic design perturbations on net thrust and HEX heat load were evaluated at cruise, maximum take-off (MTO) and ground idle (GI) operating conditions.

2. Methodology

2.1 Geometry and computational method

An in-house tool for design and analysis of engine exhaust systems was used to conduct aerothermal design analysis of the embedded HEX system. The tool consists of an automated workflow for geometry generation, meshing, solving and postprocessing of axisymmetric, separate-jet exhaust systems. The geometry generation approach uses a parametric method defined by class shape transformation (CST) functions [7]. The CST method is widely used to parameterise geometries for aerodynamic applications [13,14,15]. A CST curve is defined by the product a class function $C(x)$ and a shape function $S(x)$ with a vertical offset (Eq. 1). The axial (x) and radial (y) geometric parameters are normalised by the curve axial length (L).

$$\boldsymbol{y(x) = C(x)S(x) + x\Delta y}, \qquad \boldsymbol{x = \frac{X}{L}, y = \frac{Y}{L}} \tag{1}$$

The class function is based on the geometry of interest and varies based on requirements of the geometry to be generated. The Bernstein polynomial is used to describe the shape function (Eq. 2). The shape function is defined by the superposition of the Bernstein polynomials scaled by the coefficients A_r (Eq. 3).

$$\boldsymbol{BP_n = \sum_{r=0}^{n}(K_{r,n}x^r(1 - x^{n-r}))} \tag{2}$$

$$\boldsymbol{S(x) = \sum_{r=0}^{n}(A_r K_{r,n}x^r(1 - x^{n-r}))}, \qquad \boldsymbol{K_{r,n} = \frac{n!}{r!(n-r)!}} \tag{3}$$

Christie et al [16] combined the CST method with the PARSEC method [17] to develop the intuitive CST for use in aerodynamic design. This method allows parametric aerodynamic shapes to be created based on intuitive design variables. The iCST method was used to reduce the full engine geometry including the bypass duct and the HEX system to a set of analytical equations in the form of Eq. 1. The two-dimensional computational domain was generated with a semi-circular far-field boundary with a diameter of $75D_{MAX}$. The required boundary conditions were identified and calibrated for the desired operating conditions (Fig. 2). A fully structured multi-block meshing approach was used to generate a mesh with a y^+ of less than one. The mesh generated through this method consisted of 900,000 elements. A mesh independence study was conducted to quantify the grid convergence index (GCI) defined by Roache et al. [18]. The GCI was determined to be less than 0.5% for net thrust and HEX heat load at cruise, MTO and GI conditions.

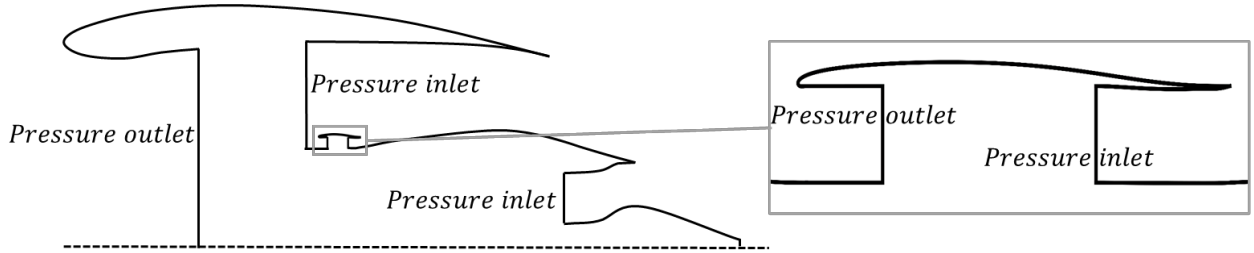

Figure 2 Boundary conditions for the engine and the HEX system.

A two dimensional implicit, axi-symmetric, compressible RANS (Reynolds Averaged Navier-Stokes) solver was used to calculate the flowfield. The density-based method was used for the high Mach number conditions of cruise and MTO while pressure based method with SIMPLE pressure-velocity coupling was used for ground idle conditions. The second order spatial discretisation was used and the gradients were computed using the Green-Gauss node-based method. The k-ω shear stress transport (SST) turbulence model was used for closure of the averaged Navier-Stokes equations [19].

2.2 HEX modelling

The HEX modelling method developed by Abdessemed et al [7] parametrically generates the embedded HEX system geometry, integrates the low order HEX model into the solver and uses the TDB method for an exhaust system with an embedded HEX. The embedded HEX system geometry is generated in a parametric manner using iCST curves. A high degree of HEX system geometry control is possible in terms of bulk system parameters including the axial and radial position of the whole system within the bypass duct. A large amount of geometric control was also possible for the subsystem components of inlet duct, outlet duct and the HEX cowl.

The coupled mixed fidelity HEX modelling method consist of an in-house workflow to model a naturally ventilated HEX system without the need of a geometry and mesh generation for the HEX. The method combines CFD with a low order model of the HEX which provides pressure loss and temperature rise across the HEX as a function of HEX mass flow. An iterative method is used to match the mass flows at the inlet and the outlet of the air side of the HEX to model a ventilated system [7]. The converged solution will provide a pressure loss and temperature rise across the HEX for a given HEX mass flow. The HEX performance maps for a range of HEX system configurations were generated using the tool detailed by Ryemill et al [8]. The tool uses empirical HEX heat transfer and pressure loss equations to evaluate the performance of a HEX system.

The predicted HEX performance for a given geometry is used to explore the sensitivity of the HEX and bypass performance to changes in HEX sizing and immersion within the bypass duct. An offset strip fin HEX was used due to the high heat transfer performance relative to the pressure loss associated with this type of HEX [20]. The Darcy-Weisbach equation quantifies the pressure loss across the HEX (Eq. 4) and Newton's law of cooling was used to calculate temperature rise (Eq. 5).

$$\boldsymbol{\Delta P_{0,HEX}} = \frac{\boldsymbol{2fL_{HEX}}}{\boldsymbol{\rho D_H}} \boldsymbol{G^2} \tag{4}$$

The pressure drop across the HEX depends on the Fanning friction factor (f), HEX length in the flow direction (L), fluid density (ρ), channel hydraulic diameter (D_H)and the flow mass flux (G).

$$\boldsymbol{\Delta T_{0,HEX}} = \frac{\boldsymbol{\varepsilon h A_{ht}(T_0 - T_w)}}{\boldsymbol{\dot{m} c_p}} \tag{5}$$

The HEX effectiveness (ε), heat transfer coefficient (h), overall heat transfer area (A_{ht}), inlet total temperature (T_0), wall total temperature (T_w), fluid mass flow rate ($\dot{m}$) and the fluid specific heat at constant pressure (c_p) determines the temperature rise across the HEX. The friction factor and the heat transfer coefficient can be calculated based on correlation from Manglik et al [21]. The friction factor is defined as:

$$f = 9.6243\,\mathrm{Re}^{-0.7422}\left(\frac{s}{h_f}\right)^{-0.1856}\left(\frac{t}{l_f}\right)^{0.3053}\left(\frac{t}{s}\right)^{-0.2659}\left[1 + 7.669\times10^{-8}\,\mathrm{Re}^{4.429}\left(\frac{s}{h_f}\right)^{0.92}\left(\frac{t}{l_f}\right)^{3.767}\left(\frac{t}{s}\right)^{0.236}\right]^{0.1} \tag{6}$$

The friction factor is defined by the fin spacing (s), fin height (h_f), fin length (l_f), fin thickness (t) and the flow Reynolds number based on channel hydraulic diameter (Re). The Colburn j factor is used to derive the Nusselt number and the heat transfer coefficient [20] as:

$$\boldsymbol{j = \frac{Nu}{RePr^{\frac{1}{3}}}} \tag{7}$$

$$\boldsymbol{h = \frac{Nuk}{D_H}} \tag{8}$$

Where Nu is the Nusselt number, Re is the Reynolds number, Pr is the Prandtl number and k is the thermal conductivity of the fluid. Manglik et al. [21] provides the correlation for the Colburn j factor in the form:

$$j = 0.6522\,\mathrm{Re}^{-0.5403}\left(\frac{s}{h_f}\right)^{-0.1541}\left(\frac{t}{l_f}\right)^{0.1499}\left(\frac{t}{s}\right)^{-0.0678}\left[1 + 5.269\times10^{-5}\,\mathrm{Re}^{1.34}\left(\frac{s}{h_f}\right)^{0.504}\left(\frac{t}{l_f}\right)^{0.456}\left(\frac{t}{s}\right)^{-1.055}\right]^{0.1} \tag{9}$$

The HEX assessment tool [8] uses fundamental pressure loss and temperature rise equations along with the empirical correlation from experiments to quantify HEX performance for a given geometry and operating condition provided to the tool. An automated method was developed to generate HEX performance maps for a range of different HEX geometries at cruise, MTO and GI operating conditions. The method also integrated the maps into the HEX modelling workflow to generate the low order HEX model. This allows rapid design space exploration and sensitivity assessment for naturally ventilated embedded HEX systems.

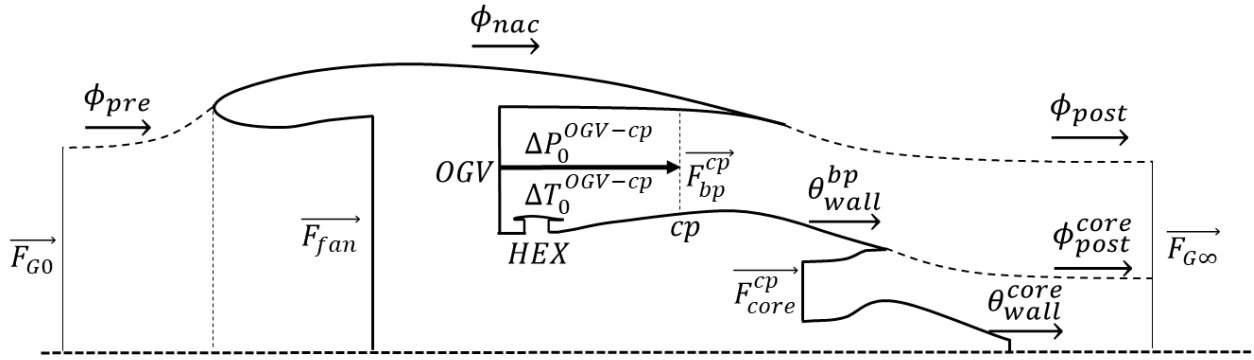

Figure 3 Thrust and Drag accounting for engine with HEX system installed within the bypass duct.

The TDB method includes the effect of HEX integration on bypass duct performance and the overall impact on net thrust (Fig. 3). The main impact of HEX integration is localised within the bypass duct and therefore two assumptions were made to quantify effect on thrust as HEX configurations were varied:

- Intake mass flow capture ratio (MFCR) is constant.
- Effect of the HEX configuration only arises within the thrust domain.

The main effects of HEX integration can be quantified using the overall net thrust:

$$\boldsymbol{F_N = F_{G\infty} - F_{G0}} \tag{10}$$

The integration of the HEX into the bypass duct introduces a blockage effect which affects the mass flow within the bypass duct. This is an artefact of the computational method which needs to be eliminated to allow consistent comparisons between different HEX system configurations. A consistent value of total pressure and total temperature at the outlet guide vane (OGV) inlet station is required in order to conduct a fair analysis of the changes in system performance. For this reason the cycle based values of mass flow, total pressure and total pressure were used for postprocessing. The pressure loss and temperature rise between the OGV and the charging plane (cp) is applied to the

cycle values at the OGV to get corrected total pressure and total temperature at the charging plane (Eq. 11). The cycle corrected total pressure and total temperature values at the charging plane can be used to calculate the corrected ideal velocity (Eq. 12).

$$\boldsymbol{P_{0,corr}^{cp} = P_0^{OGV,cycle} + \Delta P_0^{OGV-cp}}, \quad \boldsymbol{T_{0,corr}^{cp} = T_0^{OGV,cycle} + \Delta T_0^{OGV-cp}} \tag{11}$$

$$\boldsymbol{V_{ideal,corr}^{cp,cycle} = \sqrt{\frac{2\gamma R T_{0,corr}^{cp}}{\gamma-1}\left(1 - \left(\frac{p_{s,\infty}}{P_{0,corr}^{cp}}\right)\right)}} \tag{12}$$

The ideal propulsive force ($\boldsymbol{IPF_{corr}^{cycle}}$) can be calculated from the cycle corrected ideal velocity ($\boldsymbol{V_{ideal,corr}^{cp,cycle}}$) (Eq. 13)**.** The velocity coefficient ($C_{v,cp}^{\infty,CFD}$) is calculated from the CFD results and multiplied to IPF_{corr}^{cycle} to give the corrected gross propulsive force (GPF_{corr}^{cycle}) through which the net thrust can be determined (Eq. 14).

$$\boldsymbol{IPF_{corr}^{cycle} = \frac{GPF_{corr}^{cycle}}{C_{v,cp}^{\infty,CFD}} = \dot{m}_{bp}^{corr} V_{ideal,corr}^{cp,cycle} + \dot{m}_{core}^{CFD} V_{ideal}^{core} + \dot{m}_{vent}^{CFD} V_{ideal}^{vent}} \tag{13}$$

$$\boldsymbol{F_N = F_{G\infty} - F_{G0} = C_{v,cp}^{\infty,CFD} IPF_{corr}^{cycle} - \dot{m}_{intk,corr}^{cycle} V_{flight}} \tag{14}$$

2.3 Operating conditions and performance requirements

The design and integration of the HEX system should aim to minimise the detrimental impact on net thrust while ensuring the heat transfer requirement is met. The overall volume of the HEX should also be minimised in order to reduce the overall weight of the system. The effect of thrust loss associated with HEX integration can be quantified at the two operating conditions of cruise and MTO.A loss in thrust is generally compensated for through an increase in the fuel flow rate to maintain a constant overall net thrust.

At cruise condition the fuel flow rate is increased to achieve the same net thrust as a baseline case without a HEX and results in a deterioration in the specific fuel consumption (SFC). The increased fuel flow rate at MTO conditions leads to an increase in turbine entry temperature (TET) which can lead to a decrease in turbine life [22]. Ground Idle (GI) is generally a benign operating condition with low pressure ratios within the bypass duct which can lead to a low mass flow through a HEX embedded within the bypass duct. It is essential that the HEX heat transfer requirement is met at GI conditions for a ventilated embedded HEX system.

Approximate engine operating condition at cruise was provided by Giangaspero et al [23]. A freestream Mach number of 0.85 and a fan-nozzle pressure ratio (FNPR) of 2.2 was identified for an UHBR engine with a bypass ratio of over 15. Wolf et al [24] detailed that the engine operating conditions at MTO with an FNPR range of 1.3 and 1.4 for an UHBR engine operating within a Mach number range of 0 and 0.4. The benign engine operating conditions at GI can be approximated with a FNPR of 1.01 and a freestream Mach number of 0.03.

The maximum heat transfer requirement for the HEX is expected to be at MTO conditions where the engine fan rotation speeds are the highest. Nikolaidis et al. [4] estimated the heat transfer requirement or a similar UHBR engine to that considered in this paper at MTO to be approximately 150 kW. The heat transfer requirements at cruise and GI conditions were derived from the requirement at MTO condition. The fan power for the UHBP engine at MTO conditions and the heat transfer requirement at MTO can be used to estimate the efficiency of the planetary power gearbox to be 99.7%. Engine operating conditions at cruise can be used to calculate the fan power. The gearbox losses can then be estimated as a product of the gearbox efficiency and the fan power to be 55 kW at cruise. The gearbox loss estimations for GI conditions were based on the relative difference in revolutions per minute (RPM) of the low pressure (LP) turbine shaft at MTO and GI conditions. The LP shaft RPM at GI is 60% of the RPM at MTO conditions [25]. The quadratic relation between RPM and gearbox losses can be used to estimate the gearbox losses at GI to be 54 kW. Therefore, the heat dissipation requirement at GI conditions is estimated to be 54 kW. Overall, these are approximate values that are sufficient to highlight the capabilities and sensitivities of the current study.

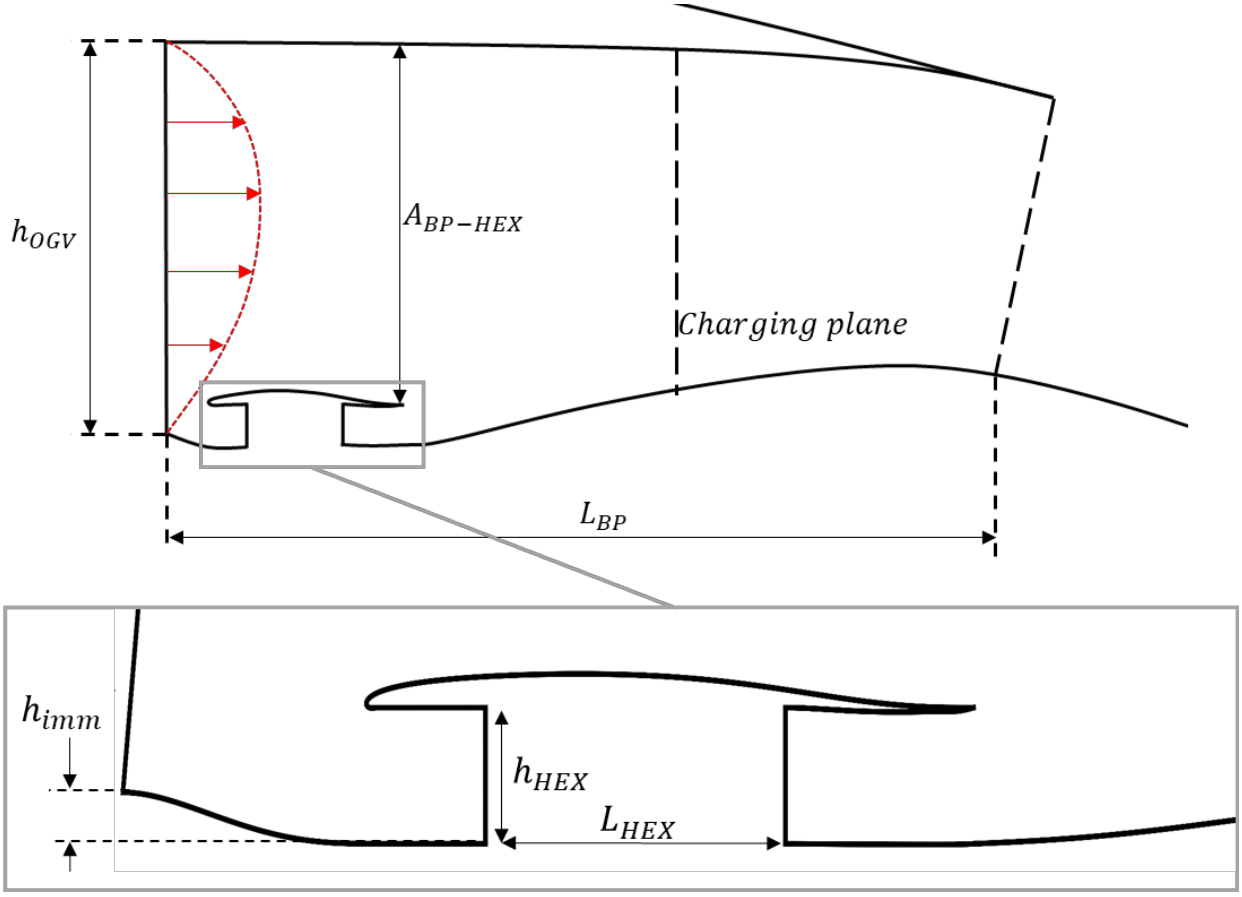

Figure 4 Main geometric parameters HEX system embedded within the bypass duct

2.4 Embedded HEX system configurations

The general aim of this paper is to demonstrate the capabilities of a coupled mixed fidelity model to model a ventilated HEX embedded within the bypass duct. The method can be used to explore the sensitivity of the HEX and bypass performance to the design and integration of the embedded HEX system. The main design parameters of interest are the length of the HEX (L_{HEX}), the height of the HEX (h_{HEX}) and the radial immersion of the HEX into the bypass duct (h_{imm}) (Fig. 4). The three design parameters control the overall size of the HEX, the air mass flux through the HEX which affects the pressure loss (Eq. 4) and total temperature rise (Eq. 5) across the HEX. The bypass duct outer aeroline radial position can be used to control the local area within the duct ($A_{BP\text{-}HEX}$) thus altering the static pressure field within the bypass duct and thereby possibly affect the massflow through the ventilated HEX. The design parameters of choice are perturbed in a full factorial manner to allow design sensitivity analysis.

3. Results and analysis

3.1 Embedded HEX system – effect of sizing

The integration of a naturally ventilated HEX system into the bypass duct introduces a pressure loss and temperature rise between the OGV and the charging plane. The sensitivity of the HEX performance in terms of heat transfer rate (Q) and the bypass performance as net thrust (F_N) to perturbations in the size of the HEX in terms of L_{HEX} and h_{HEX} were quantified at cruise, MTO and GI operating conditions. The full-factorial design space exploration study was used to identify the performance trends and design bounds within the design space (Fig. 5).

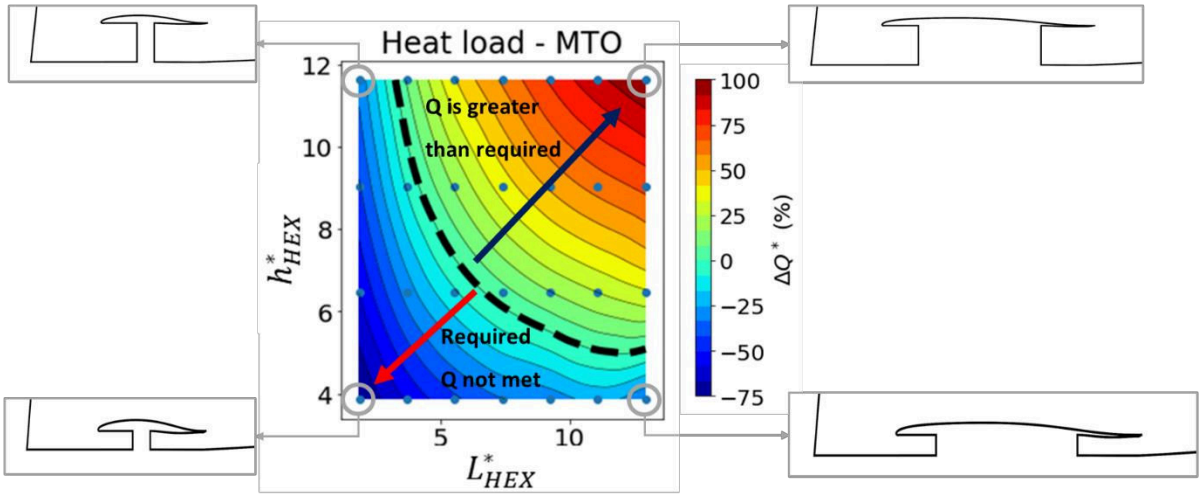

Figure 5 Map of HEX heat load variation due to change in HEX size. Black dashed line represents the design that exactly meet the HEX heat transfer requirement. Designs below the line do not meet the requirement and designs about the line exceed the requirement.

The parameters $h^*_{HEX} = h_{HEX}/h_{OGV}$ (%) and $L^*_{HEX} = L_{HEX}/L_{BP}$ (%) represent the HEX height and length non-dimensionally. Non-dimensional HEX heat transfer rate is quantified relative to the required heat transfer rate at the defined operating condition (Eq 15).

$$\boldsymbol{\Delta Q^*}(\%) = \frac{\boldsymbol{100(Q-Q_{req})}}{\boldsymbol{Q_{req}}} \tag{15}$$

Comparisons of the performance of the HEX system at cruise, MTO and GI was used to identify the dominant design bounds within the design space. The overall performance trend was as expected where an increase in L_{HEX} and h_{HEX} resulted in an increase in HEX heat transfer rate. Generally, it was found that all designs within the design space met the HEX heat requirement at cruise condition (Fig. 6). Design bounds were identified for MTO and GI conditions. For this example, the design bound for heat transfer rate at MTO condition is identified as the dominant design bound.

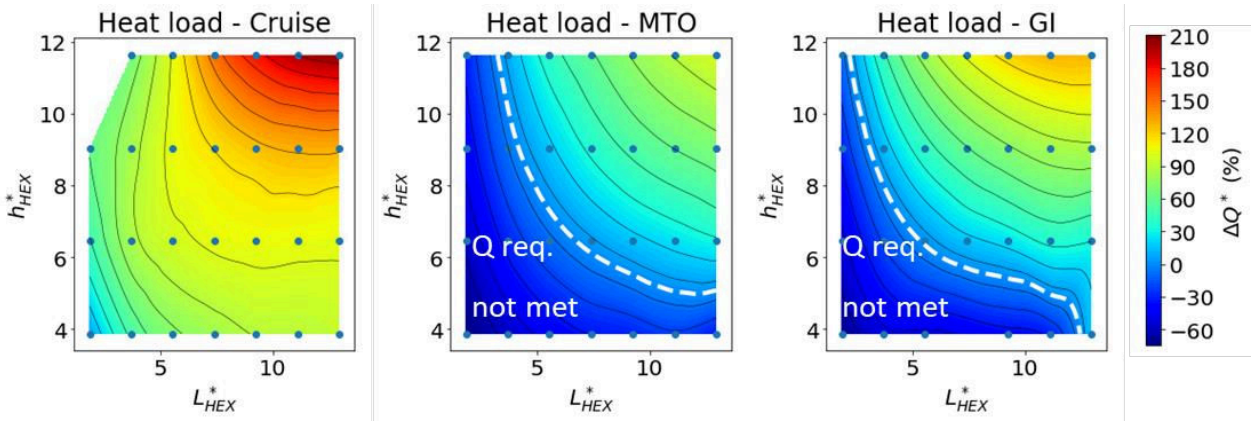

Figure 6 Variation in HEX heat transfer rate due to change in HEX size at cruise, MTO and GI conditions. White dashed line represents designs that meet the Q requirement.

A change in HEX size for a naturally ventilated system will affect the coupling between the HEX and the bypass duct. This results in a change in the mass flow rate and the mass flux across the HEX as the HEX design and integration is perturbed. Effect of HEX size on the net thrust is quantified at cruise and MTO conditions. Net thrust is not a performance parameter for GI conditions. Loss in thrust is normalised by the net thrust for a clean engine without a HEX to provide the non-dimensional parameter ΔF^*_N (Eq. 16). As expected, the larger the HEX the greater the loss in net thrust (Fig. 7), albeit with also notable changes in Q (Fig. 6). The loss in thrust was more sensitive to a change in the height of the HEX than the length of the HEX.

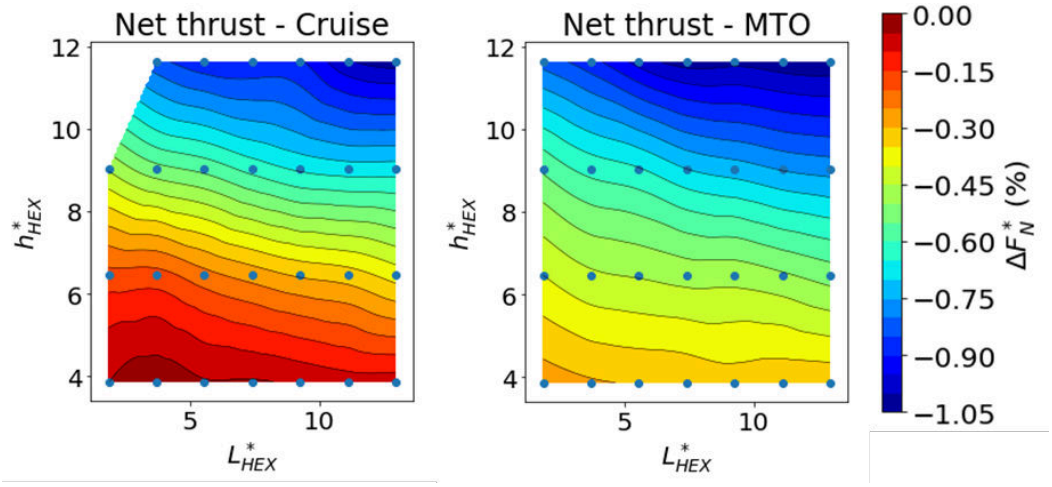

Figure 7 Net thrust map at cruise and MTO as a function of the change in HEX size.

$$\boldsymbol{\Delta F_N^*}(\%) = \frac{\mathbf{100}(\boldsymbol{F_N} - \boldsymbol{F_{N,clean}})}{\boldsymbol{F_{N,clean}}} \tag{16}$$

The pressure loss across the HEX is the dominant source of pressure loss between the OGV exit and the charging plane. The HEX system intake duct, exhaust duct and any mixing losses were an order of magnitude lower than the pressure loss across the HEX. The only source of temperature rise between the OGV exit and the charging plane is the mass weighted effect of temperature rise across the HEX. The pressure drop between the OGV and the charging plane is more sensitive to the height of the HEX than the length of the HEX (Fig. 8). The change in net thrust across the design space is mainly due to the effect of pressure loss between the OGV and the charging plane. Temperature rise between the OGV and the charging plane does not have a significant effect on the change in net thrust. This suggests that if the main objective is only to minimise the thrust loss then a HEX design with a small h_{HEX} should be selected and the sensitivity to HEX length (L_{HEX}) is relatively modest.

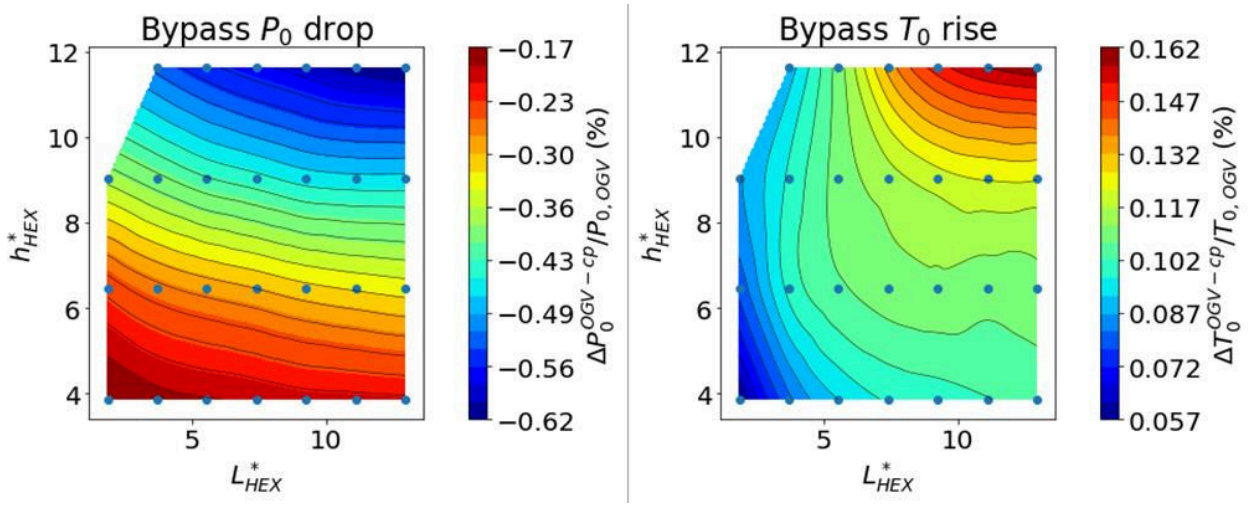

Figure 8 Map of pressure loss (left) and temperature rise (right) at cruise between the OGV and the charging plane as a function of change in HEX length and height.

The performance maps for loss in net thrust and the distribution of heat transfer across the design space can be combined into a single map to identify the main design bounds within the design space (Fig. 9). The best HEX system configuration that has the lowest thrust loss and meets the heat requirement at MTO has a thrust loss of $\Delta F_N^* = 0.28\%$ at cruise. A design bound associated with the intake separation is also identified. Intake separation is caused due to a reduction in the HEX intake mass flow capture ratio (MFCR). A low MFCR results in a captured streamtube with a high diffusion ratio. This leads to a diffusion induced separation at the HEX intake Embedded HEX systems with no intake separation should be selected in order to ensure that the effect of flow maldistribution is minimised.

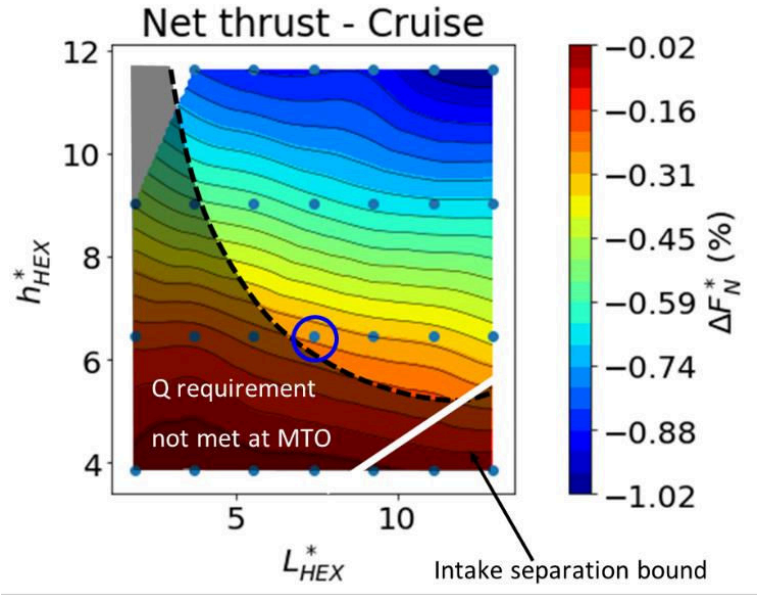

Figure 9 Map of net thrust at cruise with design bounds for heat transfer at MTO and intake separation superimposed. Design in blue circle is the best HEX system design within the design space.

The general design trend is to make a HEX with low h_{HEX} and high L_{HEX} if the aim is to only minimise thrust loss and meet the heat transfer requirement. However, the volume of the HEX should also be taken into consideration during the design process in order to minimise the potential penalties associated with the weight of the HEX and practical aspects of the integration. HEX configurations with low L_{HEX} and high h_{HEX} meet the heat transfer requirement while minimising the HEX volume (Fig. 10).

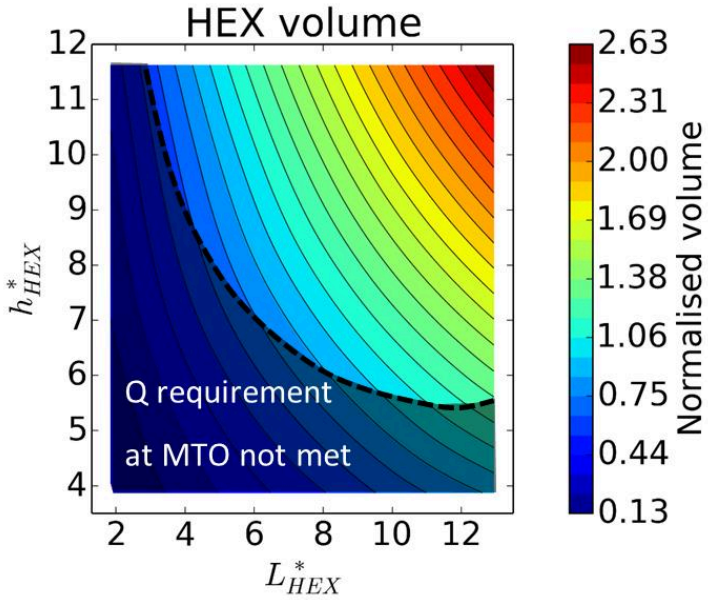

Figure 10 Map of HEX volume as a function of L_{HEX} and h_{HEX} with the heat transfer design bound at MTO superposed onto the map.

The trade-off between the loss in net thrust at cruise and the change in HEX volume for all designs that meet the heat transfer requirement at MTO condition can be summarised into a single figure (Fig. 11). Generally an increase in L_{HEX} and a decrease in h_{HEX} results in an beneficial reduction in thrust loss. Further increase in L_{HEX} results in a saturation in the effect on net thrust which leads to a large increase in HEX volume with no significant added benefit in thrust loss. Similarly, a reduction in L_{HEX} and an increase in h_{HEX} leads to designs that minimise the HEX volume while meeting the heat transfer requirements. A significant increase in h_{HEX} causes L_{HEX} to decrease at an equivalent rate in order to maintain a constant Q. This causes the HEX volume to remain constant while the thrust loss further

deteriorates. This suggests that the best HEX system designs that minimise the detrimental effects of thrust loss and volume while meeting the heat requirement is a balance between L_{HEX} and h_{HEX}.

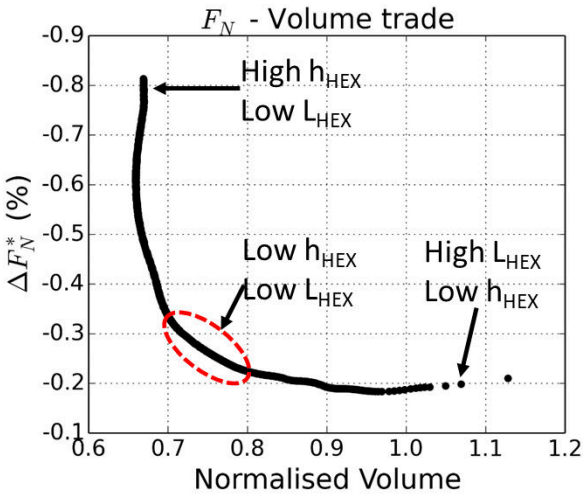

Figure 11 Trade-off between loss in net thrust at cruise and HEX volume for all HEX system designs within the design space that meet the heat requirement at MTO. Best design is within the region encircled in red.

3.2 Embedded HEX system – effect of radial immersion

One method to reduce pressure loss across a given HEX is to reduce the air mass flux through the HEX (Eq. 4) while still meeting the Q requirement. The mass flux through the HEX in a ventilated configuration depends on the effective pressure ratio between the inlet and the exit of the HEX. The pressure ratio can be controlled by changing the static pressure at the HEX cowl trailing edge. The pressure ratio and hence the HEX mass flux is likely to be dependent on the level of immersion of the HEX system into the bypass duct (Fig. 12).

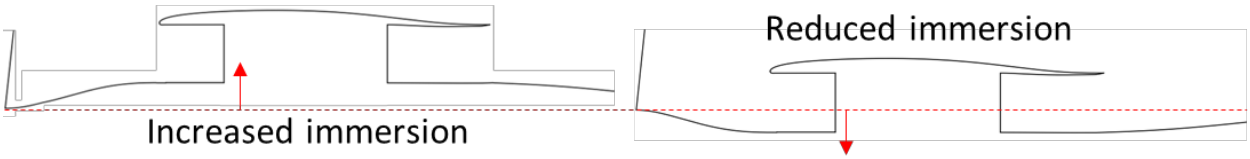

Figure 12 Immersion nomenclature: Increased immersion into bypass (left), reduced immersion into bypass (right).

A reduction in the HEX system radial immersion from $h^*_{imm} = h_{imm}/h_{OGV}$ (%) = 0% to 2.5% resulted in an improvement in cruise net thrust by 0.1% for the best designs within the design spaces (Fig. 13). Best designs are HEX system configurations that meet the heat transfer requirement without flow separation at the HEX inlet while minimising the detrimental impacts on net thrust. The separation boundary within the design space deteriorated as HEX system radial immersion was reduced.

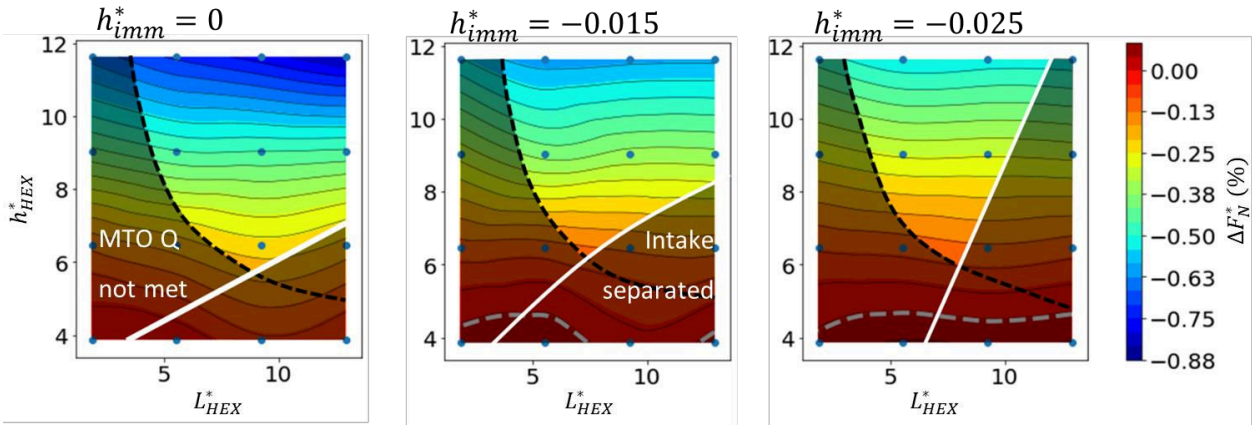

Figure 13 Thrust loss maps at cruise with MTO heat transfer design bound (black dashed line) at HEX system at three different HEX system radial immersions. Intake separation bound is defined by sloid white line.

A 1.5% reduction in the radial immersion of the HEX system into the bypass duct from $h^*_{imm} = 0$ to $h^*_{imm} = -0.015$ results in an improvement in the trade-off between net thrust and HEX volume (Fig. 14). Intake separation boundary for configurations with no radial immersion is identified at a normalised volume of 0.8. A reduction in HEX system immersion by 1.5% for the same normalised volume of 0.8 resulted in a 0.07% thrust benefit. There was no significant benefit in further reduction in h_{imm} to 2.5%. Alternatively, the reduction in h_{imm} by 1.5% allowed the volume of the HEX to be reduced by 7% while maintaining the same thrust loss and heat transfer rate.

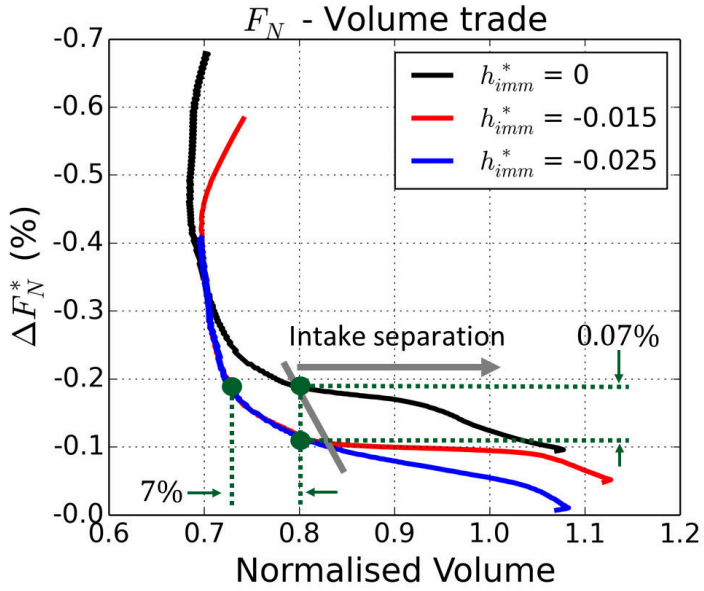

Figure 14 Change in trade-off between thrust loss at cruise and HEX volume due to change in HEX system radial immersion. Grey line indicates separation boundary.

3.3 Embedded HEX system – effect of the bypass duct outer aeroline

A reduction in the HEX system intake MFCR promotes a diffusion led separation within the intake duct. One potential method to control the intake separation is to increase MFCR of the HEX system intake duct by reducing the static pressure at the exit of HEX system outlet duct. This increases the pressure ratio across the HEX system and can increase the air mass flow through the HEX. To investigate this design aspect the radial position of the bypass duct outer aeroline was varied to control the bypass flow area ($A_{BP\text{-}HEX}$) and hence the static pressure in the region of the HEX cowl trailing edge (Fig. 15).

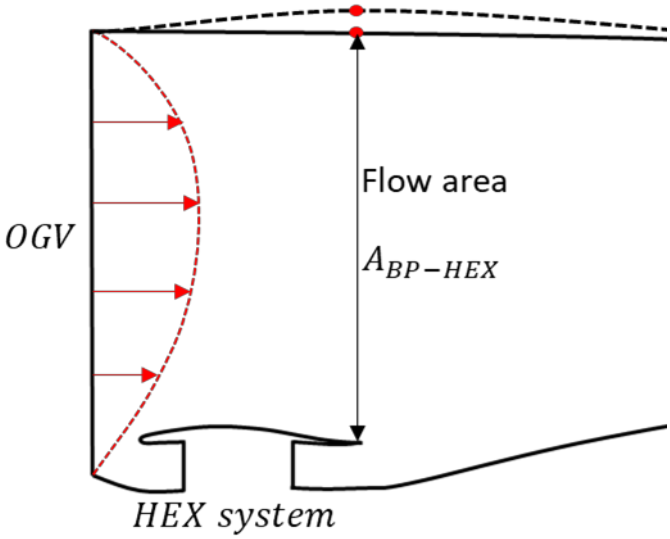

Figure 15 Control of radial position of bypass duct outer aeroline.

The increase in mass flow resulted in the reattachment of the flow within the intake and improved the separation boundary within the design space (Fig. 16). There was no significant effect of a 5% reduction in $A_{BP\text{-}HEX}$ on the design bound of the heat transfer requirement at MTO condition. However, the increase in HEX mass flow resulted in an increase in total pressure loss across the HEX and the total pressure loss between the OGV and the charging plane. This led to a deterioration in the thrust loss across the design space. There was a 0.1% deterioration in cruise thrust loss for the best designs between the baseline design with no change in bypass duct outer aeroline and design with 5% reduction in $A_{BP\text{-}HEX}$. The method can be used to improve the HEX intake separation however the penalty in the form of deterioration in net thrust is notable.

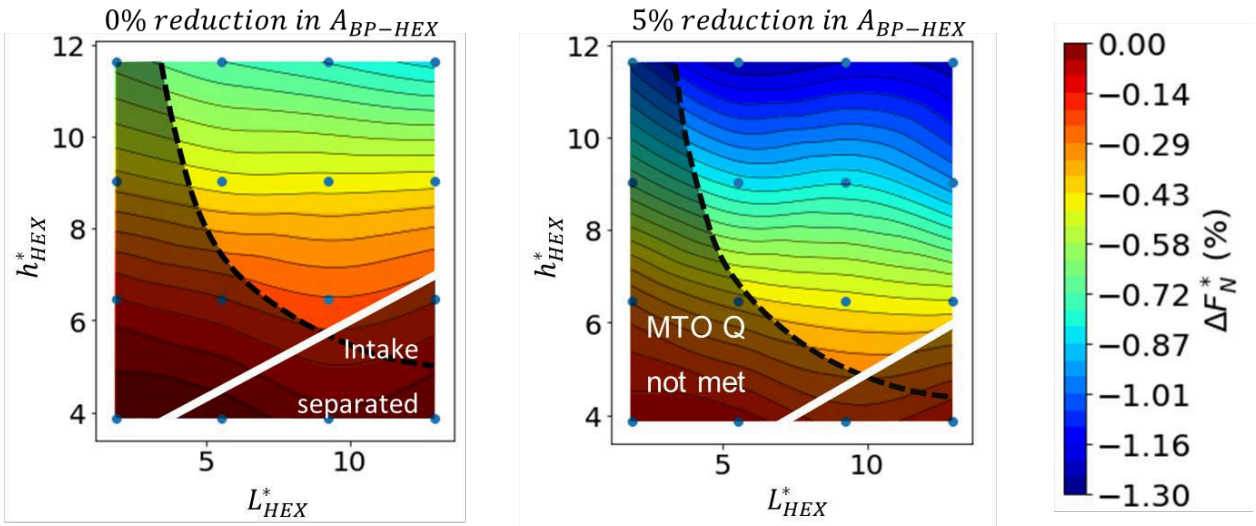

Figure 16 Effect of change in $A_{BP\text{-}HEX}$ on thrust loss maps at cruise and on design bounds for heat transfer requirement at MTO and intake separation.

4 Conclusions

A general method has been developed to explore the effect of variations in HEX design and installation on the net thrust, heat load and HEX volume. The method can be used to identify the regions of the design space which contain the best design and installation configurations. The best designs are defined as designs that meet the heat requirements at the smallest HEX volume and with minimum detrimental impact on net thrust.

For the configurations explored, it was identified that the best HEX design and installation depended on both the length and the height of the HEX. This was because a HEX that meets the required heat load at MTO with a high

L_{HEX} and low h_{HEX} was generally beneficial for net thrust at cruise. However HEX configurations with high h_{HEX} and low L_{HEX} generally has a lower overall volume.

The pressure loss across the HEX was identified as the main source of thrust loss. The reduction in radial immersion of the HEX system into the bypass duct was identified as a method to reduce the mass flux through the HEX and reduce the pressure loss across the HEX. A 1.5% reduction in the radial immersion of a HEX system with a normalised volume of 0.8 resulted in a 0.07% improvement in thrust loss. The 1.5% reduction in h_{imm} allows the HEX volume to be decreased by 7% while maintaining a constant thrust loss and HEX heat transfer rate. The HEX intake separation boundary within the design space deteriorates as the HEX system radial immersion is decreased. Methods that use local momentum injection or momentum transfer should instead be used to increase mixing near the separated region and control the local flow to eliminate separation the intake separation. Relative to current methods the contribution of this work is to demonstrate the capability of the coupled mixed fidelity method to model a ventilated HEX system within the bypass duct. The method can be used to conduct rapid design assessments and allow design sensitivity studies for embedded HEX systems.

Acknowledgements

The author is partially funded by the UK Research and Innovation Engineering and Physical Sciences Research Council (EPSRC) under project reference 2268554. Significant contribution has been provided by Abdessemed et al. [7] who was partially funded by UK Research and Innovation under project reference 113263.

References

[1] Cao, H., Z.G. Zhou, X.L. Ye. 2021. Aerodynamic characteristic comparison of ultra-highly and normally loaded fans, *The Aeronautical Journal*, Vol. 125, No. 1293

[2] Larsson, L., T. Gronstedt and K. G. Kyprianidis. 2011. Conceptual design and mission analysis for a geared turbofan and an open rotor configuration, *Turbo Expo: Power for Land, Sea, and Air*, Vol. 54617, pp. 359–370

[3] Kyprianidis, K. G., T. Gronstedt, S. O. T. Ogaji, P. Pilidis and R. Singh. 2010. Assessment of Future Aero-engine Designs With Intercooled and Intercooled Recuperated Cores, *Journal of Engineering for Gas Turbines and Power* 133 (1), 011701.

[4] Nikolaidis, T., S. Jafari, D. Bosak and P. Pilidis. 2020. Exchange rate analysis for ultra high bypass ratio geared turbofan engines, *Applied Sciences* 10 (21) 7945.

[5] Li, H., H. Huang, G. Xu, J. Wen and H. Wu. 2017. Performance analysis of a novel compact air-air heat exchanger for aircraft gas turbine engine using LMTD method, *Applied Thermal Engineering* 116, 445–455.

[6] Goulos, I., T. Stankowski, D. MacManus, P. Woodrow and C. Sheaf. 2018. Civil turbofan engine exhaust aerodynamics: Impact of bypass nozzle after-body design, *Aerospace Science and Technology*, 73, 85-95.

[7] Abdessemed, C. 2023. Cranfield internal communications.

[8] Ryemill, M., C. Bewick and J. Kee Min. 2016. The Rolls-Royce PLC UltraFan heat management challenge, *30th Congress of the International Council of the Aeronautical Sciences*., ICAS 2016_0344

[9] Goulos, I., T. Stankowski, J. Otter, D. MacManus, N. Grech and C. Sheaf. 2016. Aerodynamic design of separate-jet exhausts for future civil aero-engines, part 1: Parametric geometry definition and CFD approach, *ASME J. Eng. Gas Turbines and Power* 138, (8), 081201.

[10] Goulos, I., J. Otter, T. Stankowski, D. MacManus, N. Grech and C. Sheaf. 2016. Aerodynamic design of separate-jet exhausts for future civil aero-engines, part 2: Surrogate modeling and optimization, *ASME J. Eng. Gas Turbines and Power* 138, (8), 081202.

[11] Goulos, I., J. Otter, T. Stankowski, D. MacManus, N. Grech and C. Sheaf. 2018. Design optimisation of separate-jet exhausts for the next generation of civil aero-engines, *The Aeronautical Journal* 122 (1256), 1586–1605.

[12] Goulos, I., T. Stankowski, D. MacManus, P. Woodrow and C. Sheaf. 2018, Civil turbofan engine exhaust aerodynamics: Impact of bypass nozzle after-body design, *Aerospace Science and Technology* 73, 85–95.

[13] Kulfan, B. M. 2010. Recent extensions and applications of the CST universal parametric geometry representation method. *Aeronaut. J*. 114:157-176

[14] Lane, K. A. and D. D. Marshall. 2010. Inverse airfoil design utilizing CST parameterization. In: *48th AIAA Aerospace Sciences Meeting Including the New Horizons Forum and Aerospace Exposition*. 1-14.

[15] Christie, R., A. Heidebrecht and D. MacManus. 2017. An automated approach to nacelle parameterization using intuitive class shape transformation curves. *J. Eng. Gas Turbines Power*. 139:1-9.

[16] Christie, R., M. Robinson, F. Tejero and D. G. MacManus. 2019. The use of hybrid intuitive class shape transformation curves in aerodynamic design. *Aerospace Science and Technology*. 95:1-13.

[17] Sobieczky, H. 1999. Parametric airfoils and wing (Chapter), in: *Notes on Numerical Fluid Mechanics*, vol. 68, Vieweg Verlag, pp. 71–87.
[18] Roache, P. J. 1994. Perspective: A method for uniform reporting of grid refinement studies. *Journal of Fluids Engineering*, 116(3), 405–413
[19] Menter, F. T. 1994. Two-equations eddy-viscosity turbulence models for engineering applications. *AIAA Journal*. 32:1598-1605
[20] Shah, R.K., and Sekulic, D.P. 2003, Chapter 7.5.3.1 Offset strip fins in: *Fundamentals of Heat Exchanger Design*, pp:516
[21] Manglik, R. M. and Bergles, A.E. 1995, Heat transfer and pressure drop correlations for the rectangular offset strip fin compact heat exchanger, *Experimental Thermal and Fluid Science*, Vol. 10, Issue 2, pp: 171-180
[22] Cumpsty, N.A. 2015. Part 1, Chapter 5.3 Turbine inlet temperature in: *Jet propulsion: A simple guide to the aerodynamic and thermodynamic design and performance of jet engines*, pp: 65
[23] Giangaspero, G., D. MacManus and I. Goulos. 2019, Surrogate models for the prediction of the aerodynamic performance of exhaust systems, *Aerospace Science and Technology*, 92, 77–90
[24] de Wolf, W. B. 1996. Possibilities and limitations of VHBR and UHBR turbofan simulations in engine/airframe integration wind tunnel experiments, NLR TP 96028 U, National Aerospace Laboratory NLR, Amsterdam, The Netherlands.
[25] Kumar, B., DeRemer, D. and Marshall, D. 2004. Ground Idle in: *An Illustrated Dictionary of Aviation*, pp:320

2023-07-13

Heat exchanger integration with an aero-engine bypass duct

Bajimaya, Raul

Council of European Aerospace Societies (CEAS)

Bajimaya R, MacManus DG, Abdessemed C, et al., (2023) Heat exchanger integration with an aero-engine bypass duct. In: Aerospace Europe Conference Joint 10th EUCASS - 9th CEAS Conference 2023, 9-13 July 2023, Lausanne, Switzerland

https://www.eucass.eu/conferences-and-publications/conference-papers